AN INVESTIGATION INTO THE EFFICACY OF RADIOTHERAPY PROTOCOLS FOR THE TREATMENT OF LUNG CARCINOMA AND THE OPTIMIZATION OF DOSIMETRY CALCULATIONS

Tareg Mohammed Al Mansour [1], Hassan saleh Al khamsan [2], Ibrahim Ali Alsulaiman [2],Mohammed Husaain Alyami [3], Mohammed Mahdi Alajmi [4], SALEH RAJEH ALYAMI [5]

Article History: Received: 20.05.2022 **Revised:** 10.07.2022 **Accepted:** 15.08.2022

Abstract

The search for efficient treatment options is necessary since lung cancer is still a major global health concern. In order to better understand how radiation treats lung cancer, this study looked at how dose distribution is affected by lung tissue heterogeneity.

Supplies and Procedures: There were two parts to the study's methodology. First, therapy setups and procedures were established using a computerized treatment planning system. Then, in order to evaluate dosage fluctuations, experimental data were collected using ionization chambers inside a phantom. The study included sophisticated lung cancer treatment planning methods that took dynamic variations in lung density into consideration.

To assess dosage estimations, Collapsed Cone Convolution Superposition (CCCS) was used, taking into account variables such relative lung density, treatment geometry, and dose comparisons.

Findings: According to analysis, CCCS-based computations showed dosage homogeneity within 1% of adaptive convolution (AC) doses. This suggests that AC is a good substitute because of its faster processing speed.

In summary, the research shows that the CCCS algorithm in the treatment planning system can accurately calculate doses, including for heterogeneous media like lung tissue. The accuracy of CCCS in taking tissue density variations into account is confirmed by Monte Carlo calculations.

Keywords: Low-density materials, heterogeneous media, dose calculation, radiotherapy, lung cancer, small cell lung cancer, and non-small cell lung cancer.

1 Medical Physicist in New Najran General hospital
2 Radiological Specialist in New Najran General Hospital
3 Radiographer Technologist in New Najran General Hospital
4 Radiological Technologist in King Khaled Hospital
5 RADIOLOGICAL SPECIALIST In ABQAIQ GENERAL HOSPITAL

DOI: 10.53555/ecb/2022.11.12.308

Introduction:

The most common disease worldwide, primarily affecting males, is lung cancer, which develops in the lungs or pulmonary parenchyma and is the leading cause of cancer-related death in both sexes. In Australia, where it is one of the top four diagnosed diseases, the incidence of lung cancer has skyrocketed in recent years, with a 13% increase in 2015 over 2012. These frightening rates have been reached. Lung cancer is mostly caused by smoking, which accounts for around 80% of cases. However, there are other risk factors that are associated with lung cancer as well, such as genetic predispositions, occupational exposures, dietary variables, and air pollution. consists of two primary subtypes: non-small cell lung cancer (NSCLC), which accounts for most cases and has different clinical features from small-cell lung cancer (SCLC). NSCLC, which includes adenocarcinoma, large-cell undifferentiated carcinoma, and squamous cell carcinoma, frequently advances slowly, delaying the identification of symptoms until later stages. Lung cancer has a dismal prognosis even with improvements in therapeutic approaches that include surgery, systemic

treatments, palliative care, and interventional radiology, especially in advanced stages.

It becomes clear that radiotherapy is an essential therapeutic approach that works for all patient performance levels and illness stages. Nevertheless, the difficulties associated with thoracic radiation therapy, such as tumor mobility caused by respiration and heartbeat, low lung tissue electron density, and close proximity to vital anatomical systems like the esophagus and spinal cord, limit its effectiveness. Promising ways to get around these challenges are provided by advanced radiation technologies, which will improve treatment results. However, radiation is still underutilized worldwide, which calls for a thorough assessment of its clinical utility—especially given the rising cost of healthcare.

With an emphasis on dosage adjustments made necessary by lung tissue heterogeneity, this study intends to investigate the role of radiation therapy in the treatment of lung cancer. This research aims to optimize radiotherapeutic approaches for the treatment of lung cancer through careful analysis.

Supplies and Procedures:

There were two primary components to the methods used in this investigation. First, a computerized treatment planning system (TPS) was used to create setups and procedures. Afterwards, a phantom setup with ionization chambers as the baseline was used to collect experimental data.

The TPS procedure is as follows:

The University of Wollongong assisted in the use of the Pinnacle 3 treatment planning framework from Philips Healthcare in this investigation. The treatment plan included a dose grid with a matrix granularity of 2 mm, covering a width and depth of 25 cm. The lung phantom had a variable density ranging from 5 to 15 cm deep, POI3 had a density of 20 to 25 cm, and POI1 had a density of 1 g/cm³ at a depth of 5 cm. The 6MV and 10MV radiation intensities were used with a 100 cm Source-to-Surface Distance (SSD). Field sizes ranged from 3 x 3 cm to 10 × 10 cm in order to take dose delivery into consideration.

Various phantom densities (0.1, 0.2, 0.3, and 0.4 gm/cm³) were used in experiments to evaluate the impact of density fluctuation on dosage calculation. Understanding photon interactions with different densities—which is essential for precise dosage calculations—was achieved through the analysis of mass attenuation and absorption coefficients. Simulated were field widths of 6 MV energy and densities of 10 MV energy. Important configurations for later procedures were saved for additional examination.

Experimental Methodology:

A Varian 21Ex Linear Accelerator (LINAC) was used in the experiments at Wollongong Hospital, and ionization chambers were used to evaluate dose fluctuations. Initial steps included rotating the collimator, gantry, table, and laser to make sure the LINAC settings satisfied treatment requirements. The readings were normalized to a standard SSD of 100 cm. The solid water phantom was positioned at the isocenter, and ionization chambers were positioned at different depths and field widths.

The absorbed dose in the heterogeneous lung phantom was measured along the center axis using a CC04 conventional ionization chamber. Depth measurements were obtained by varying the distances and applying energies of 6MV and 10MV across field widths of 3 cm x 3 cm, 5 cm x 5 cm, and 10 cm x 10 cm. To ensure accuracy in treatment planning calculations, a comparison was done between the projected dosages by the Pinnacle3 treatment planning system and the measured dosages using ionization chambers.

Techniques for Calculating Doses:

The dose calculation in this study was done using Pinnacle3, a 3D treatment planning program. To determine the lung tissue dosage distribution, the Collapsed Cone Convolution Superposition (CCCS) algorithm was specifically utilized. With the inclusion of secondary electrons, heterogeneity issues within lung regions, and primary photon interactions, the CCCS model allows for precise estimate of three-dimensional dose distributions. Most notably, the CCCS method makes it possible to determine the dose distribution in areas impacted by electrical imbalances, including the lung's air cavities.

Dose Model with Convolution Superposition:

Based on the methods described by Mackie et al., Pinnacle3's CCCS dosage algorithm emphasizes first-principles computations without the need for correction factors in order to estimate dose allocation. Dose distribution calculations using this model take patient

contours, tissue inhomogeneity, and radiation modulation into account.

The method starts by splitting incident photons coming from the accelerator head into smaller units. Then, as the energy center crosses the patient's sample density, the Total Energy Released per unit Mass (TERMA) volume is calculated. Ray-tracing methodology is used to trace the heterogeneity and lateral scatter effects over the energy deposition kernel of the TERMA in three dimensions. In light of the sudden attenuation and electron mediation, the estimated photon dose allocation is finally modified.

Superposition of Adaptive Convolution:

Pinnacle3 also uses the Adaptive Convolution Superposition (ACS) technique, which improves computation techniques without sacrificing dose calculation accuracy. The TERMA is assessed in conjunction with dosage distribution on a rough 3D grid. Greater curvature zones receive high-resolution dose allocation, while higher curvature regions receive dynamic resolution upgrades. On the other hand, the coarse grid provides the dose distribution in areas with reduced curvature. The ACS technique shortens computation times without sacrificing the accuracy of CCCS when taking tissue heterogeneities into consideration. Together, these techniques provide accurate and effective dose computation inside the framework of treatment planning, which is critical for maximizing the effectiveness of radiotherapeutic treatments in the management of lung cancer.

Results and Graph Discussions

Radiotherapy planning requires careful consideration of the depth-dose characteristics for different lung densities at 6 and 10 MV energies, as well as variable field dimensions. These features provide important information for maximizing treatment efficacy and reducing side effects by illuminating how dose distributions change with lung tissue density and treatment parameters.

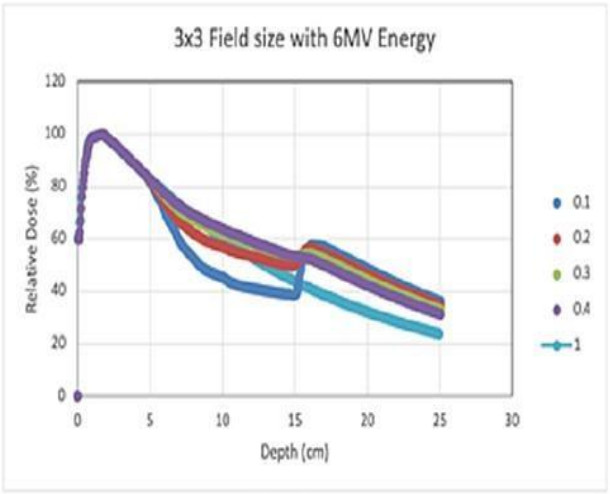

(2; a)

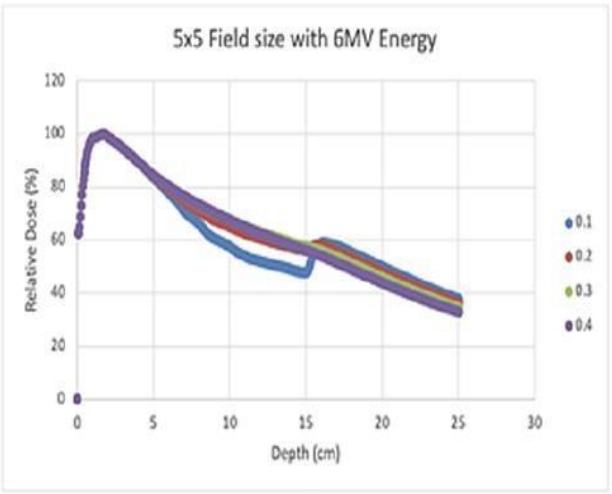

(2; b)

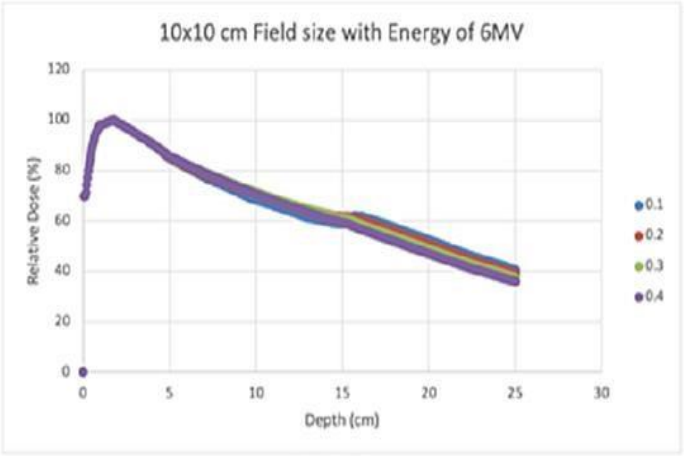

(2; c)

The depth-dose characteristics for various lung densities at 6 MV are shown in Figure 2, taking into account various field dimensions. The relative dose proportion is plotted against depth in cm on the graph. At the surface of the phantom down to a depth of 5 cm, water, with a density of 1 g/cm³, replicates the density of the human body.

The graph includes many curves that represent lung densities at depths of 5 to 15 cm, with values ranging from 0.1 to 0.4 g/cm³. Furthermore, the area between 15 and 25 cm is the peripheral body tissue, which is primarily made up of water with a density of 1 g/cm³. For the purpose of optimizing radiotherapeutic interventions in the treatment of lung cancer, these depth-dose characteristics offer vital insights into the patterns of dose distribution inside lung tissue of different densities.

The lung tissue, which is a medium with a lesser density, showed a more noticeable decline in percentage. Proportionate dosage reduction happened as density dropped, with 0.1 g/cm³ showing the lowest proportional dose. The trend for 0.2 g/cm³, 0.3 g/cm³, and 0.4 g/cm³ was similar, but the absorption slope of the latter two showed a small shift in comparison to the water medium.

With a field size of 5 cm by 5 cm, Figure 2(b) shows the depth-dose characteristics for various lung densities at 6MV. In the water medium (1 g/cm³), the patterns are still evident, but in the lung medium (0.1 g/cm³), the discrepancies are more pronounced.

The depth-dose characteristics at 6MV with a field dimension of 10cm × 10cm are shown for different lung densities (0.1 g/cm³, 0.2 g/cm³, 0.3 g/cm³, and 0.4 g/cm³). It is clear that a bigger field dimension of 10 cm × 10 cm and uniform delivery of 6MV radiation intensity have no effect on density fluctuations in the lung tissue.

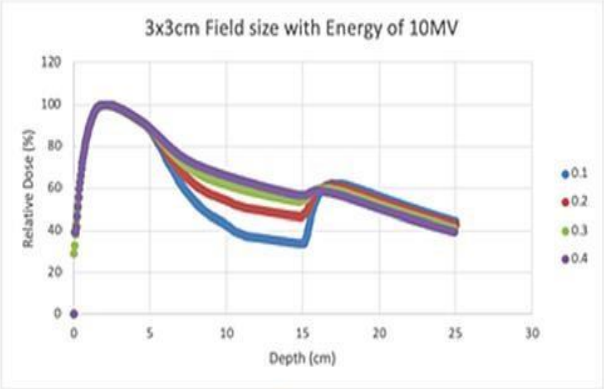
3x3cm Field size with Energy of 10MV
Relative Dose (%)
Depth (cm)
0.1
0.2
0.3
0.4

(3; a)

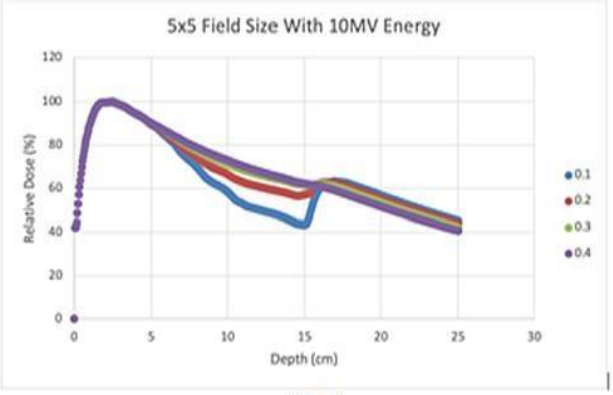
5x5 Field Size With 10MV Energy
Relative Dose (%)
Depth (cm)
0.1
0.2
0.3
0.4

(3; b)

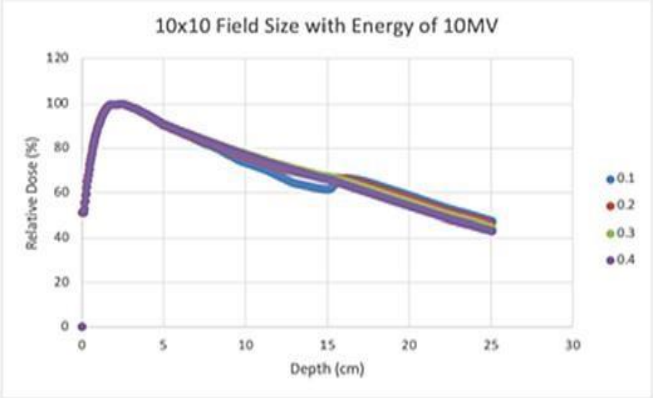
10x10 Field Size with Energy of 10MV
Relative Dose (%)
Depth (cm)
0.1
0.2
0.3
0.4

(3; c)

The depth-dose characteristics for various lung densities at 10 MV are shown in Figure 3, taking into account varying area dimensions.

For a field dimension of 3 cm × 3 cm, the depth-dose characteristics for lung densities ranging from 0.1 g/cm³ to 0.4 g/cm³ are shown in Figure 3(a). At 0.1 g/cm³, there is a significant drop in absorption in the lung medium. Nevertheless, absorption characteristics were not present in the lung and lower body mediums for densities of 0.3 g/cm³ and 0.4 g/cm³.

With a field dimension of 5 cm × 5 cm, Figure 3(b) shows the depth-dose characteristics for the identical lung densities. In the lung medium, lower absorption percentages are seen at densities of 0.1 and 0.2 g/cm³. Nonetheless, variations in absorption ratio were not statistically significant for concentrations of 0.3 and 0.4 g/cm³.

The depth-dose characteristics for a field dimension of 10 cm by 10 cm are displayed in Figure 3(c). An absorption ratio pattern for the densities is seen, with the exception of 0.1 g/cm³ in the lung medium, where absorption percentages were decreased.

For the purpose of optimizing radiotherapeutic treatments in the treatment of lung cancer, these findings offer important insights into the effects of treatment parameters and lung tissue density on dose distribution characteristics.

The results from the Treatment Planning System (TPS) with a radiation energy of 6MV with a field dimension of 5 cm x 5 cm as the baseline are compared in this section using the Collapsed Cone Convolution Superposition (CCCS) algorithm and Ionization Box Assessment. This comparison is shown in Figure 4(b). 0.3 g/cm³ was found to be the typical density used for 6MV energy radiation via Pinnacle3. For the research, a 5% accuracy margin was kept.

The findings showed that Pinnacle3 and the ionization chamber were consistent at all depths, and that the heterogeneous phantom had an average density of 0.3 g/cm³. Figure 4(a) compares results for a heterogeneous phantom subjected to a 6MV radiation intensity through a 3cm × 3cm field, using the same density of 0.3 g/cm³. Comparing results for a 6MV beam intensity assaulted over a 10cm x 10cm field, Figure 4(c) does the same.

In all cases, the calculated dose using the CCCS computing method was in good agreement with the standard error of the ionization chamber at all depths of observation, indicating the validity of this approach for the purposes of the investigation.

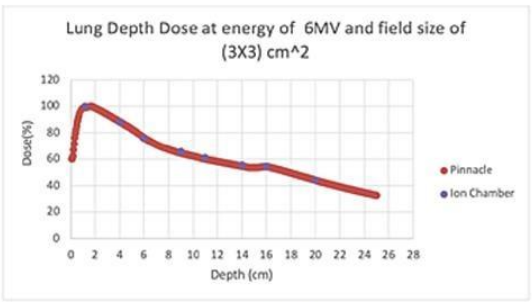

(4; a)

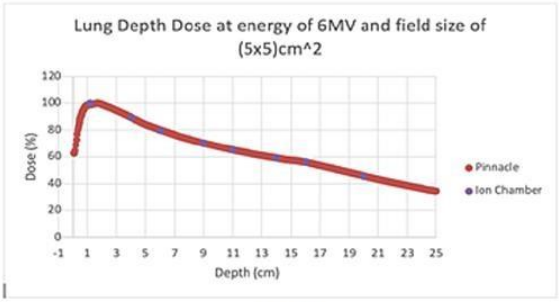

(4; b)

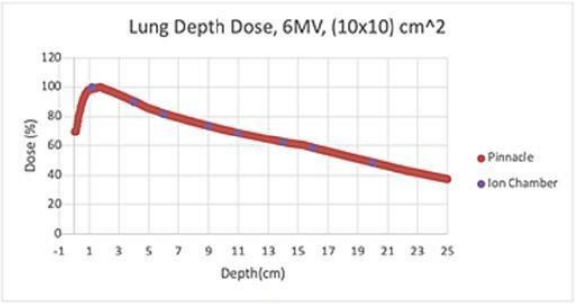

(4; c)

The graph shows that the results for the phantom with heterogeneous low-density media differed slightly from one another. As a result, there was a slight difference found between the Pinnacle3 results and the ionization chamber results. The contrast of results with a field dimension of 5 cm by 5 cm is shown in Figure 5(b). With a small deviation

at depths of 14 and 16 cm, where the actual result was marginally higher than the CCCS simulation results, the low-density media generally accords with the CCCS assessment at all levels. This test was performed with a heterogeneous material density of 0.3 g/cm³, a field dimension of 5 cm × 5 cm, and a beam intensity of 10MV.

The findings of the ionization chamber and the CCCS simulation are compared for a beam intensity of 10MV given through a field dimension of 10 cm x 10 cm in Figure 5(c). Pinnacle3's results and those from the ionization chamber agreed at every depth.

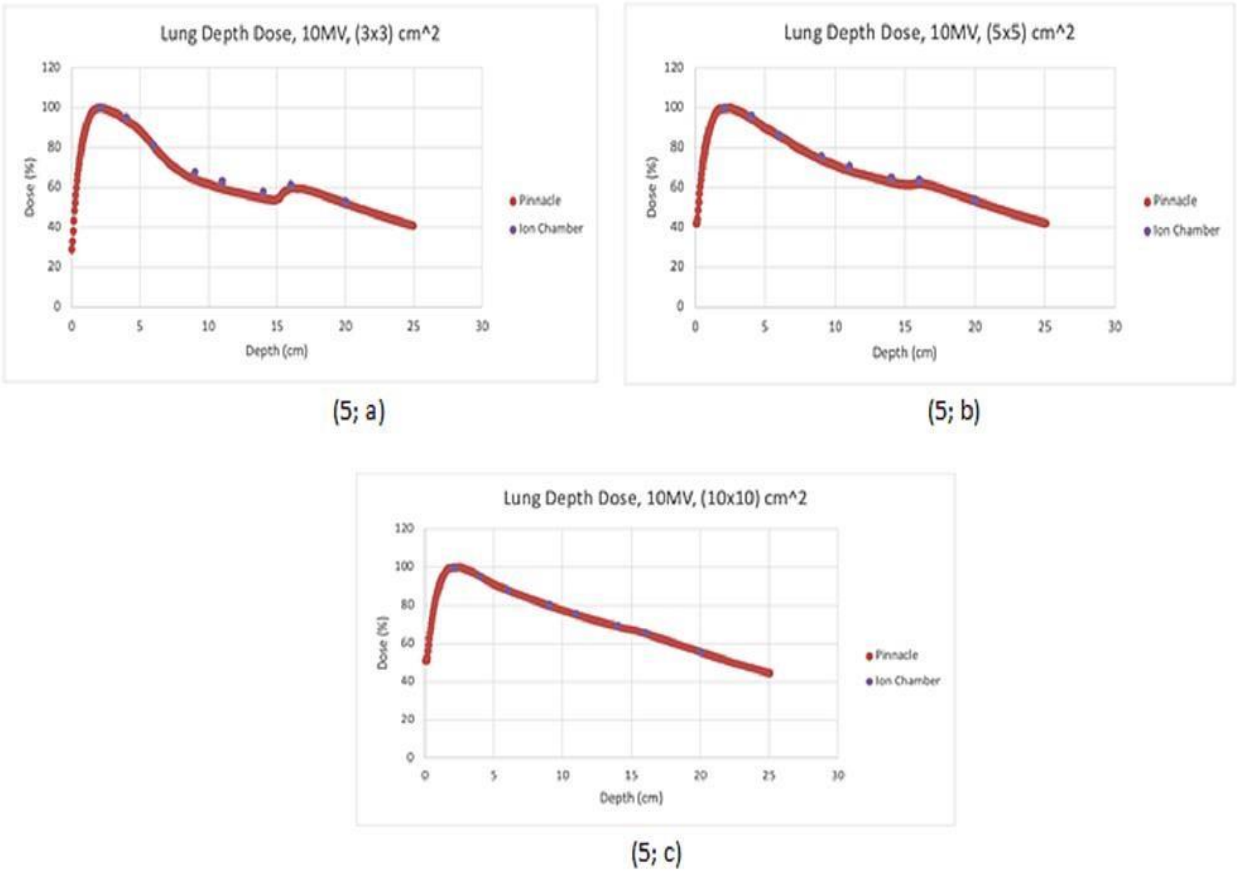

Figure 5: Findings from the treatment planning simulation Pinnacle3 CCCS and the benchmark ionization chamber are compared at different field diameters and the same radiation energy of 10MV.

(5; a): Comparison of results at the same radiation energy of 10MV and field dimension of 3cmx3cm between the treatment planning simulation Pinnacle3 CCCS and the benchmark ionization chamber.
(5; b): Comparison of results at the same radiation energy of 10MV and field dimension of 5cm x 5cm between the treatment planning simulation Pinnacle3 CCCS and the benchmark ionization chamber.
(5; c): Comparison of results at the same radiation energy of 10MV and field dimension of 10cm x 10cm between the treatment planning simulation Pinnacle3 CCCS and the benchmark ionization chamber.

The graph shows that the results for the phantom with heterogeneous low-density media differed slightly from one another. As a result, there is a small difference between the results obtained from the ionization chamber and Pinnacle 3. The low-density media generally agrees with the CCCS assessment at all levels, with the exception of depths of 14 and 16 cm, where there is a slight inaccuracy and the observed result is marginally greater than the CCCS simulation findings. The comparison of findings for a field dimension of 5 cm x 5 cm is shown in Figure (5; b). This test was performed with a heterogeneous material

density of 0.3 g/cm³, a field dimension of 5 cm × 5 cm, and a beam intensity of 10MV.

The comparison of the ionization chamber results with the CCCS simulation is shown in Figure (5; c) utilizing a 10MV beam intensity given through a field dimension of 10 cm x 10 cm. Pinnacle3's results and those from the ionization chamber agreed at every depth.

A comparison of isodose curves for three different field sizes (3cm x 3cm, 5cm x 5cm, and 10cm x 10cm) with a heterogeneous density of 0.3 g/cm³ and beam energy of 6MV is shown in Figure 6. For every field size, a symmetrical dosage profile with smooth curves over the penumbra region was seen. Nevertheless, the profile's flatness was lost at the boundaries of the 3 cm by 3 cm and 5 cm by 5 cm field sizes. There was a comparatively little total variance of about 5% in the penumbra. Furthermore, there were only minor variations, about 20%, in the Off-axis Ratio (ORA)% between the 3 cm x 3 cm and 5 cm x 5 cm measurements.

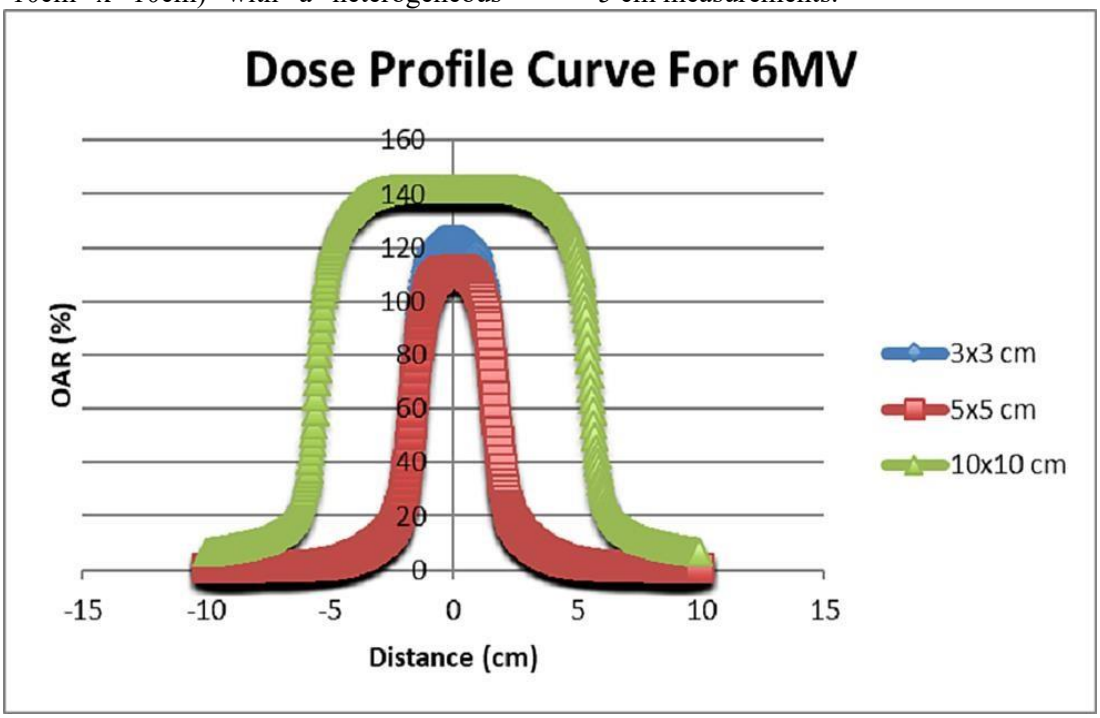

With a heterogeneous density of 0.3 g/cm³, the dose profile curves in Figure 7 were created for field sizes of 3 cm x 3 cm, 5 cm x 5 cm, and 10 cm x 10 cm with the same beam energy of 10MV. The penumbra area was smooth throughout, but the profile's flatness was only lost at the 10 cm by 10 cm field size. Across the Y-axis, a symmetrical dosage profile was noted for each of the three field sizes. The difference in Off-axis Ratio (ORA)% between 3cm x 3cm and 5cm x 5cm was greater, at roughly 40%, whereas the fluctuation profile observed in the penumbra was smaller, at about 10%.

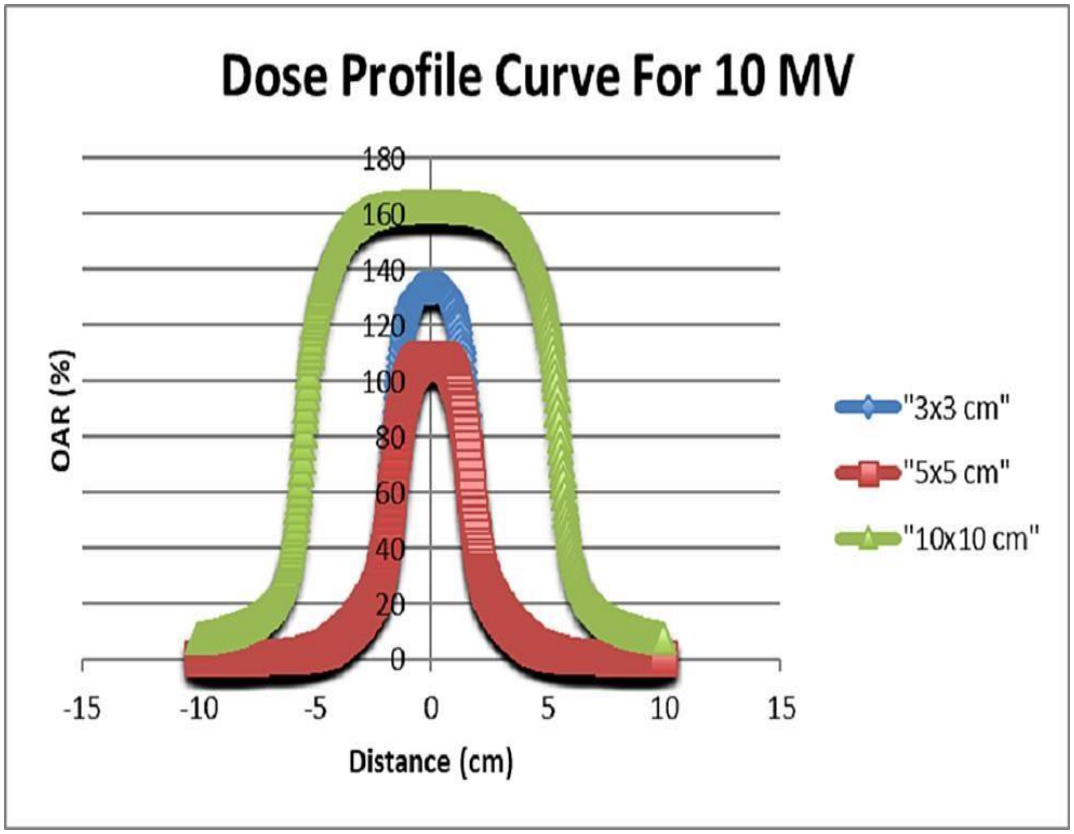

Figure 8 shows the irradiation of field sizes of 3 cm x 3 cm, 5 cm x 5 cm, and 10 cm x 10 cm using a 6MV beam of energy.

The lung medium was located between 5 and 15 cm in depth, and it had a heterogeneous density of 0.3 g/cm³. The 10cm x 10cm and 5cm x 5cm field sizes showed negligible increases in absorbed dosages, however the 3cm x 3cm field size showed a little variation in absorbed dose.
A comparison of various field widths under a 6MV beam energy and 0.3 g/cm³ density is shown in Figure 8.
The relative dosage absorbed as a percentage against depth is shown in Figure 9. 10MV was used to irradiate the lung media, which had a heterogeneous density of 0.3 g/cm³ and was situated between 5 and 15 cm below the surface. There are many curves displayed for every field size. The 10cm × 10cm field size has no discernible impact, whereas the 5cm x 5cm field size shows a somewhat tiny impact. In contrast, when viewed via the lung phantom, the 3 cm by 3 cm field size shows a notable influence of absorption.

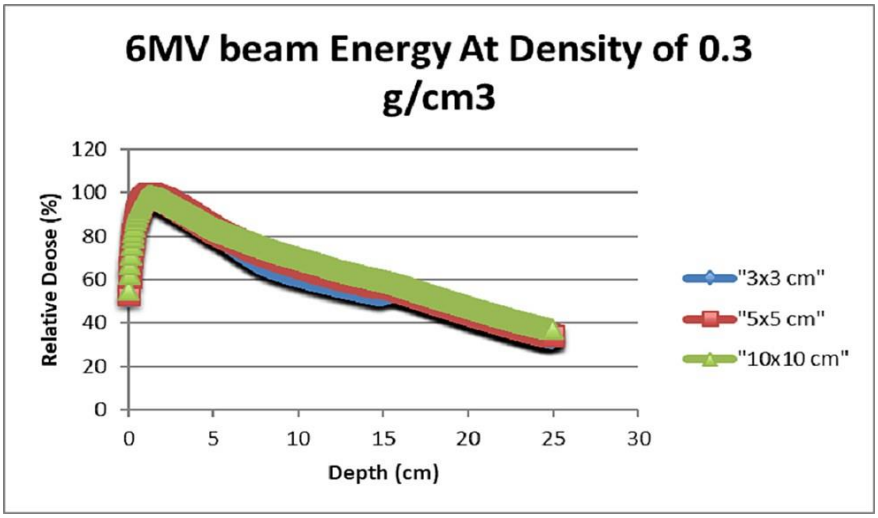

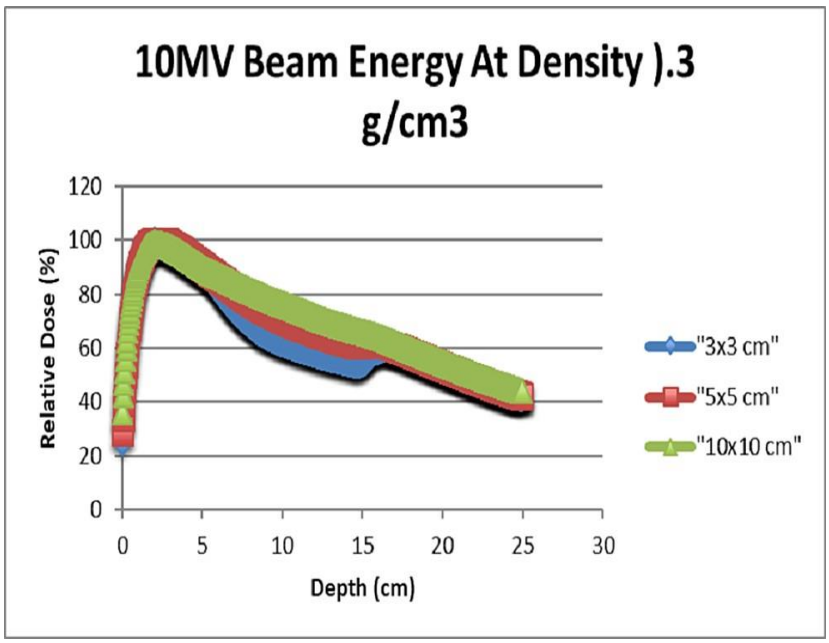

Figure 9: Comparison of different field diameters at the same density (0.3g/cm3) and beam energy (10MV).

CCCS was utilized to compare the relative absorption against depths for 6MV and 10MV pinnacles 3. Figure 10 shows the outcome of the comparison using constants, which were a heterogeneous density of 0.3 g/cm3 and a field size of 3 by 3 cm. The decline in dose absorption for 6MV pinnacle3 begins before to reaching the lung medium, which is located between the depths of 5 cm and 15 cm, respectively, as shown in figures 2–9. The dose absorption for the 6MV beam energy rose, if marginally, at the end of the lung medium, which is approximately 15 cm in depth. The decline began at a depth of about 2 cm and continued from there. When 10 MV beam energy was used, the dose absorption declined starting at a depth of about 4 cm, reaching its maximum at 15 cm. After that, it slightly increased to 16 cm, and then it continued to fall for the rest of the graph.

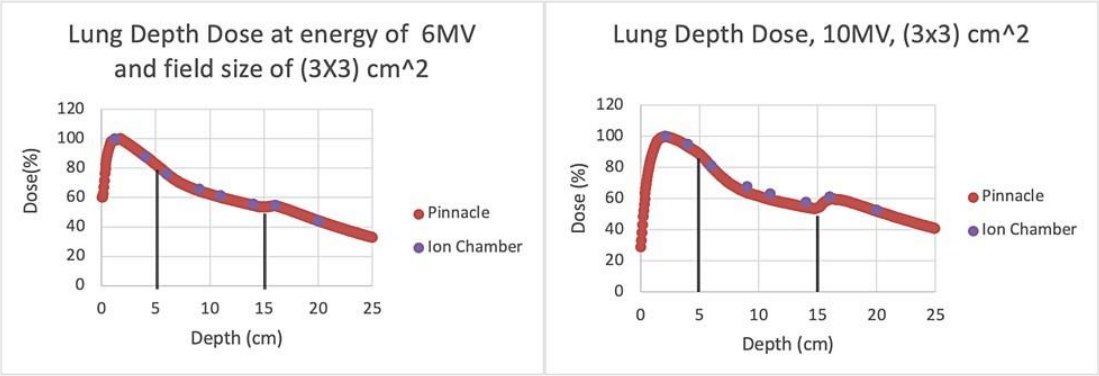

Figure 10 compares two energies, 6MV and 10MV, with the same field size and density (three centimeters by three centimeters; 0.3 g/cm3).

The heterogeneous density of 0.1 g/cm3 was the variable in the comparison of the same beam energies of 6MV and 10MV, respectively, for the same field size of 3x3 cm, as shown in figure 11. The absorption of the dose for both the 6MV and 10MV began to decrease at a depth of roughly 2 cm, reaching its lowest point in the lung medium between 5 and 15 cm. The beam energy entered the aqueous medium as soon as it reached a depth of 15 cm. The absorption of dose for both beam energies increased until a depth of 16 cm, at which point it began to fall.

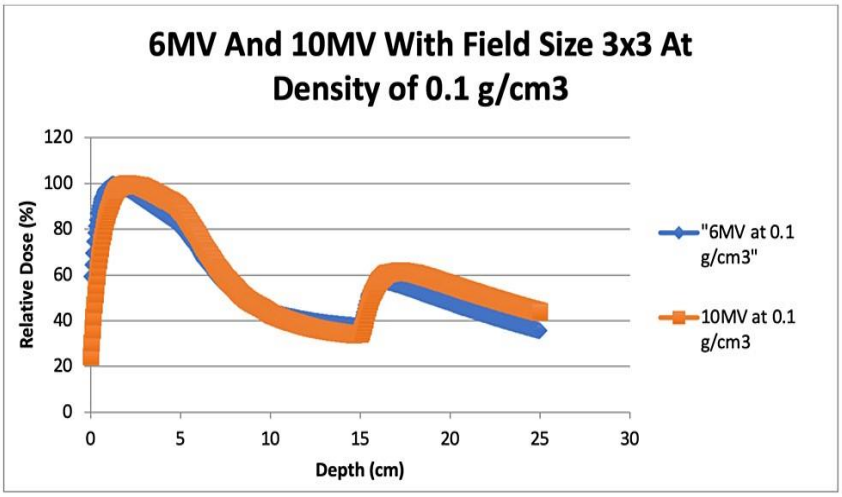

In Figure 11, the two energies (6MV and 10MV) are compared with the same field size (3 cm × 3 cm) and density (0.1 g/cm3).

Energy-related results from the CCCS and the Ionization Chamber are compared.

A 6MV pinnacle3 was compared to a 10MV pinnacle3, and a CCCS at a 6MV ionization chamber was compared to a CCCS at a 10MV ionization chamber in Figure 18. The 3x3 cm field size and the 0.3 g/cm3 heterogeneous density were the constants in this comparison. The dose found at the 6MV ionization chambers and the dose absorbed at the 6MV pinnacle3 were identical. The absorbed dose displayed at 10MV of the ionization chamber did not match the dose absorbed at 10MV pinnacle3. Furthermore, at first, there was a minor discrepancy between the 10MV ionization chamber and the 10MV pinnacle3, which diminished as the beam energy passed through the lung media.

The method employed a depth that was chosen to be 10.99 cm CCCS, as shown in Table 1. A center point of 11 cm CCCS was also applied. This position was chosen because it was in the middle of the lung phantom and fell inside the 0.3g/cm3 heterogeneous density.

	Pinnacle3			**Experimental**		
	3x3 cm	5x5 cm	10x10 cm	3x3 cm	5x5 cm	10x10 cm
6MV	60.1	65.1	68.9	61.2	65.4	68.7
10MV	59.4	68.5	75.1	63.0	70.7	75.6

Table 1 shows the percentage of dose absorbed at the closest depth point to the middle (10.99 cm) in the lung phantom using Pinnacle 3's simulation and the percentage of dose absorbed at the closest depth point to the middle (11 cm) using ionization chamber measurements.

The following formula illustrates how the dose readings from the CCCS and the ionization chamber differ, and table 2 tabulates the results.

Dose Different%= Dion-ch - D conv x100/ Dion-ch

	% Dose difference		
	3x3	5x5	10x10
6MV	1.681675	0.334618	-0.28896
10MV	5.828941	3.026936	0.54621

Table 2: Correspondence between the TPS Pinnacle 3 computation and the ionization chamber measurements from Table 1